ADVANCED MATERIALS

Supporting Information

for *Adv. Mater.*, DOI: 10.1002/adma.201904580

Engineered Fibrillar Fibronectin Networks as Three-Dimensional Tissue Scaffolds

*Stacy Jordahl, Luis Solorio, Dylan B. Neale, Sean McDermott, Jacob H. Jordahl, Alexandra Fox, Christopher Dunlay, Annie Xiao, Martha Brown, Max Wicha, Gary D. Luker, and Joerg Lahann**

Supporting Information

Engineered Fibrillar Fibronectin Networks as Three-Dimensional Tissue Scaffolds

*Stacy Jordahl, Luis Solorio, Dylan B. Neale, Sean McDermott, Jacob H. Jordahl, Alexandra Fox, Christopher Dunlay, Annie Xiao, Martha Brown, Max Wicha, Gary D. Luker, Joerg Lahann**

Supporting Text

Materials (continued from Experimental Section)

Poly(*D*,*L*-lactide-co-glycolide) or PLGA (85:15, MW 50,000 – 75,000 g/mol), chloroform, *N*,*N*-dimethylformamide, Triton X-100, Tox-8 mitochondrial activity kit, poly(*m*-phenylenevinylene)-*alt*-(2,5-dihexyloxy-*p*-phenylenevinylene)] (PMPDHPV) a fluorescent blue polymer dye, poly[tris-2,5-bis(hexyloxy)-1,4-phenylenevinylene)-*alt*-(1,3-phenylenevinylene)] (PTDPV) a fluorescent green polymer dye, anti-human fibronectin antibody, and 4'6-diamidino-2-phenylindole (DAPI) were purchased from Sigma Aldrich and used as received. Dulbecco's Modified Eagle Medium (DMEM), non-essential amino acids (NEAA), antibiotic-antimycotic, Micro-BCA kit, Dulbecco's Phosphate Buffered Saline (DPBS), human fibronectin (Corning, Corning, NY), rat tail Collagen Type I (Corning, Corning, NY), mouse laminin (Life Technologies, Carlsbad, CA) were obtained from Fisher Scientific and used as received. Siliconized low-retention microcentrifuge tubes by Biotix were purchased from VWR. Aldehyde dehydrogenase activity assay kit was obtained from Cayman Chemicals (Ann Arbor, MI) and used as received. Deoxycholic acid, sodium salt, 99% extra pure was purchased from Acros Organics. DyLight antibody labeling kit was purchased from Thermo Scientific. Stainless steel scaffold frames were custom fabricated by Microphoto, Inc. (Roseville, MI).

The following antibodies were purchased through Fisher Scientific and used as received: PE-EpCAM clone EBA-1 (BD Bioscience, San Jose, CA), APC-CD44 clone G44-26 (BD Bioscience, San Jose, CA), PE-Cy7-CD24 clone ML5 (Biolegend, San Diego, CA), mouse Pe-IgG1 clone X40 (BD Bioscience, San Jose, CA), mouse Pe-Cy7-IgG1 clone X40 (BD Bioscience, San Jose, CA), mouse APC-IgG1 clone X40 (BD Bioscience, San Jose, CA), Biotin-CD45 clone HI30 (eBioscience, San Diego, CA), Biotin-HLA-DR clone LN3 (eBioscience, San Diego, CA), Biotin-CD14 clone 61D3 (eBioscience, San Diego, CA), Biotin-CD31 clone WM59 (eBioscience, San Diego, CA), Biotin-CD41 clone MEM-06

(Abcam, Cambridge, MA), Biotin-CD19 clone HIB19 (eBioscience, San Diego, CA), Biotin-CD235a clone HIR2 (eBioscience, San Diego, CA), Biotin-CD56 clone CMSSB (eBioscience, San Diego, CA), Biotin-CD3 clone UCHT1 (eBioscience, San Diego, CA), Biotin-CD16 clone eBioCB16 (eBioscience, San Diego, CA), Biotin-CD140b clone 18A2 (Biolegend, San Diego, CA), anti-cellular fibronectin clone Fn-3 (Abcam, Cambridge, MA), anti-fibronectin mouse monoclonal IST-9 (Abcam, Cambridge, MA).

Supporting Table

Table S1. Breast cancer patient information. Fourteen breast cancer patients supplied samples from either ascites or pleural effusions to this study. Patients ranged in age, cancer type, primary tumor receptor status, and metastases. All patient samples were successfully expanded *in vitro* on fFn networks.

Patient[a)]	Sample type[b)]	Patient age	Receptor status[c)]			Detected metastases
			ER	PR	HER2	
A - IDC	AC	47	-	-	-	Lymph node, Bone
B - ILC	AC	76	+	+	-	Peritoneum, Bone
C - ILC	AC	54	+	+	+	Peritoneum, Bone
D - ---	AC	73	----	----	----	Renal, Omental, Peritoneum
E - IDC	AC	61	+	+	-	Endometrial, Uterine cancer
F - IDC	AC	51	-	-	+	Chest wall, Skin, Left axilla, Lymph node
G - IDC	PE	51	+	+	+	Skin, Pleura, Bone
H - IBC	PE	44	-	-	+	Pleura
I - IBC	PE	53	+	+	-	Chest wall, Ovaries, Bone
J - IDC, ILC	PE	57	+	-	-	Liver, Bone
K - IDC	PE	56	+	+	-	Skin, Liver, Lung, Pleura, Lymph node
L - IDC	PE	42	+	+	-	Leptomeningeal, Eye, Bone
M - IDC	PE	40	-	-	+	Lymph node
N - IDC	PE	62	+	+	-	Bone

[a)]Patient: Patient sample labelled with an arbitrary letter name followed by cancer type: invasive ductal carcinoma (IDC), invasive lobular carcinoma (ILC), inflammatory breast cancer (IBC)
[b)]Sample type: ascites (AC), pleural effusion (PE)
[c)]Receptor status: estrogen receptor (ER), progesterone receptor (PR), human epidermal growth factor receptor 2 (HER2)

Supporting Figures

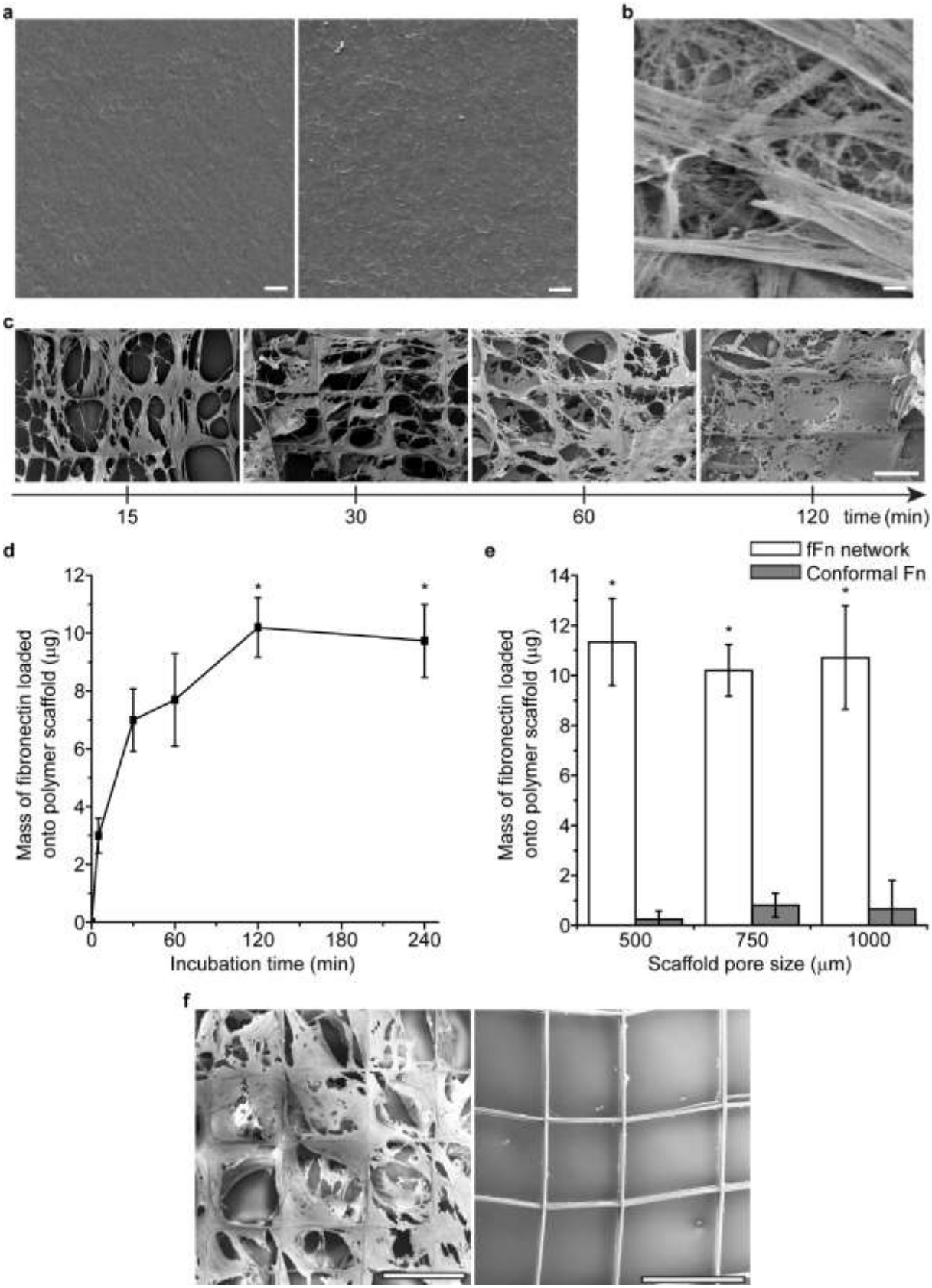

Figure S1. Shear flow at a three-phase interface with a tessellated support is needed for fibrillar fibronectin architectures and high protein loading. (a) *(right)* Fn hydrodynamically deposited onto tissue culture polystyrene (TCPS) results in minimal

fibrillogenesis while *(left)* static adsorption of Fn onto TCPS at best results in a conformal coating. Scale bars 1 μm. (b) In contrast, networks of fibrillar Fn freely suspend within the pores of a tessellated porous scaffold as a result of hydrodynamically induced fibrillogenesis. Scale bar 1 μm. (c) Time course depicting fFn loading onto the scaffold after 15, 30, 60, and 120 minutes of shearing at the three-phase interface at 30ºC. Scale bar 500 μm. (d) Mass of fFn deposited onto scaffold after 15, 30, 60, 120 and 240 minutes of hydrodynamically induced fibrillogenesis. Stars indicate no statistical difference between the 120 and 240 minute time points; 120 minutes was selected as the incubation time in the final fFn network protocol. $P<0.05$ (e) Mass of fibronectin loaded onto scaffolds is not a function of scaffold pore size after either hydrodynamically induced fibrillogenesis (fFn networks, white bars) or conformal coating via static adsorption (grey bars). Stars indicate no statistical difference amongst the protein masses loaded onto scaffolds of three different pore sizes; stars also indicate that mass loadings from all hydrodynamically deposited protein (white bars) are statistically different from the conformal coatings (grey bars). $P<0.05$ (f) SEM contrasting Fn loading and distribution when *(left)* hydrodynamically deposited and *(right)* statically adsorbed onto tessellated scaffolds. Scale bars 500 μm.

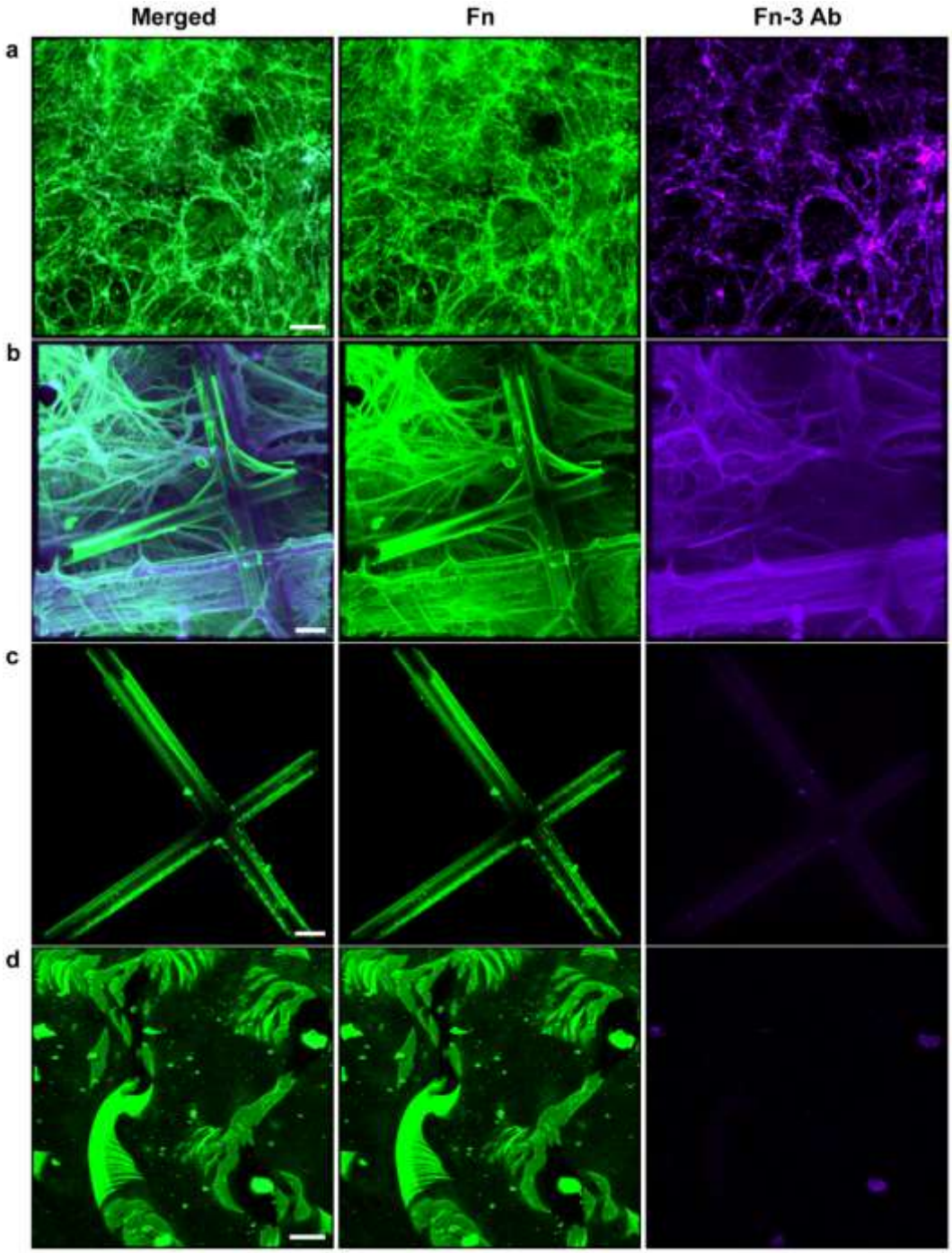

Figure S2. Antibody staining after hydrodynamically induced fibrillogenesis versus statically adsorbed fibronectin. (a) Fn (green) as secreted by human mammary fibroblasts cultured on glass and subsequently decellularized revealing the presence of cellular Fn as stained by the Fn-3 antibody (purple). Overlay of the two channels shown in left column. (b-d) *(left)* Overlay of channels, *(center)* fibronectin (green), and *(right)* cellular Fn as identified by Fn-3 antibody (purple). Fibronectin is deposited (b) onto a tessellated scaffold via hydrodynamically induced fibrillogenesis to form a fFn network, and conformally deposited onto (c) a tessellated scaffold and (d) glass. Scale bars 25 μm. All images taken at the same laser power and imaging settings via LSCM. Strong overlap of green and purple appear white in overlay image *(left images in (a) and (b)).* Saturated pixels in the Fn-3 Ab channel of *(a)* appear pink in color.

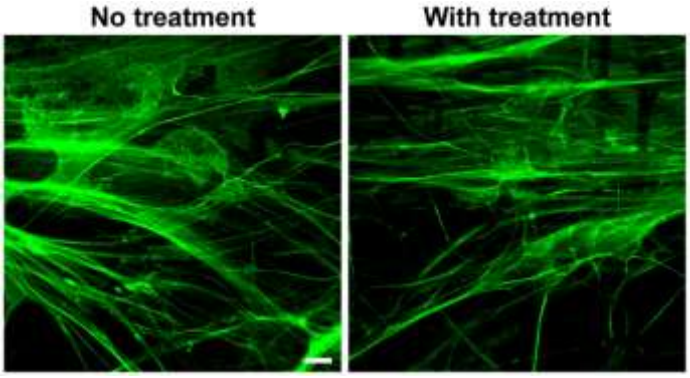

Figure S3. fFn networks remain intact after deoxycholate treatment. *(Left)* Fn (green) deposited by hydrodynamically induced fibrillogenesis onto a tessellated scaffold. *(Right)* Fn (green) deposited by hydrodynamically induced fibrillogenesis onto a tessellated scaffold after 1% deoxycholate treatment. Scale bar 50 μm.

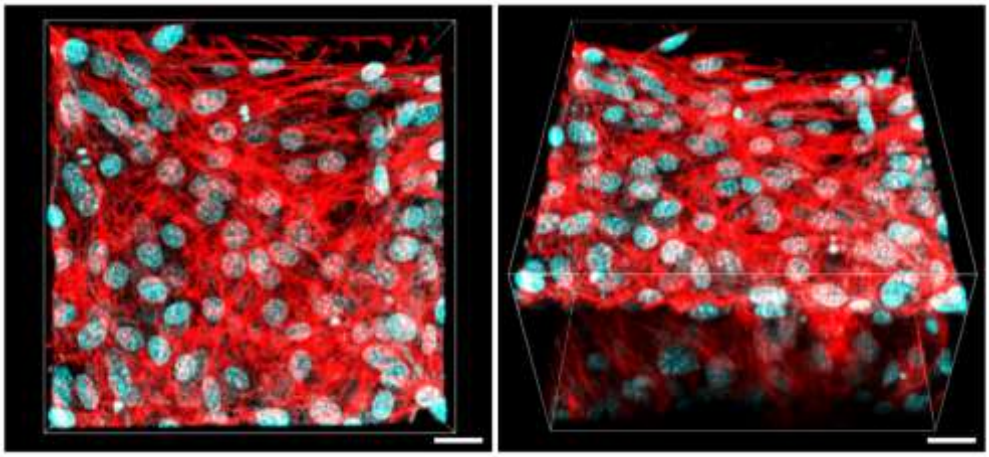

Figure S4. fFn networks enable rapid formation of 3D interconnected cell-cell contacts. NIH-3T3 mouse fibroblasts cultured three days on fFn networks result in elements multiple cell layers thick at a depth of 126 μm. *(left)* Top view and *(right)* tilted view of NIH-3T3 fibroblasts within the 500 μm square pore of the tessellated scaffold. Channels: cyan, cell nucleus; red, actin. Scale bar 25 μm.

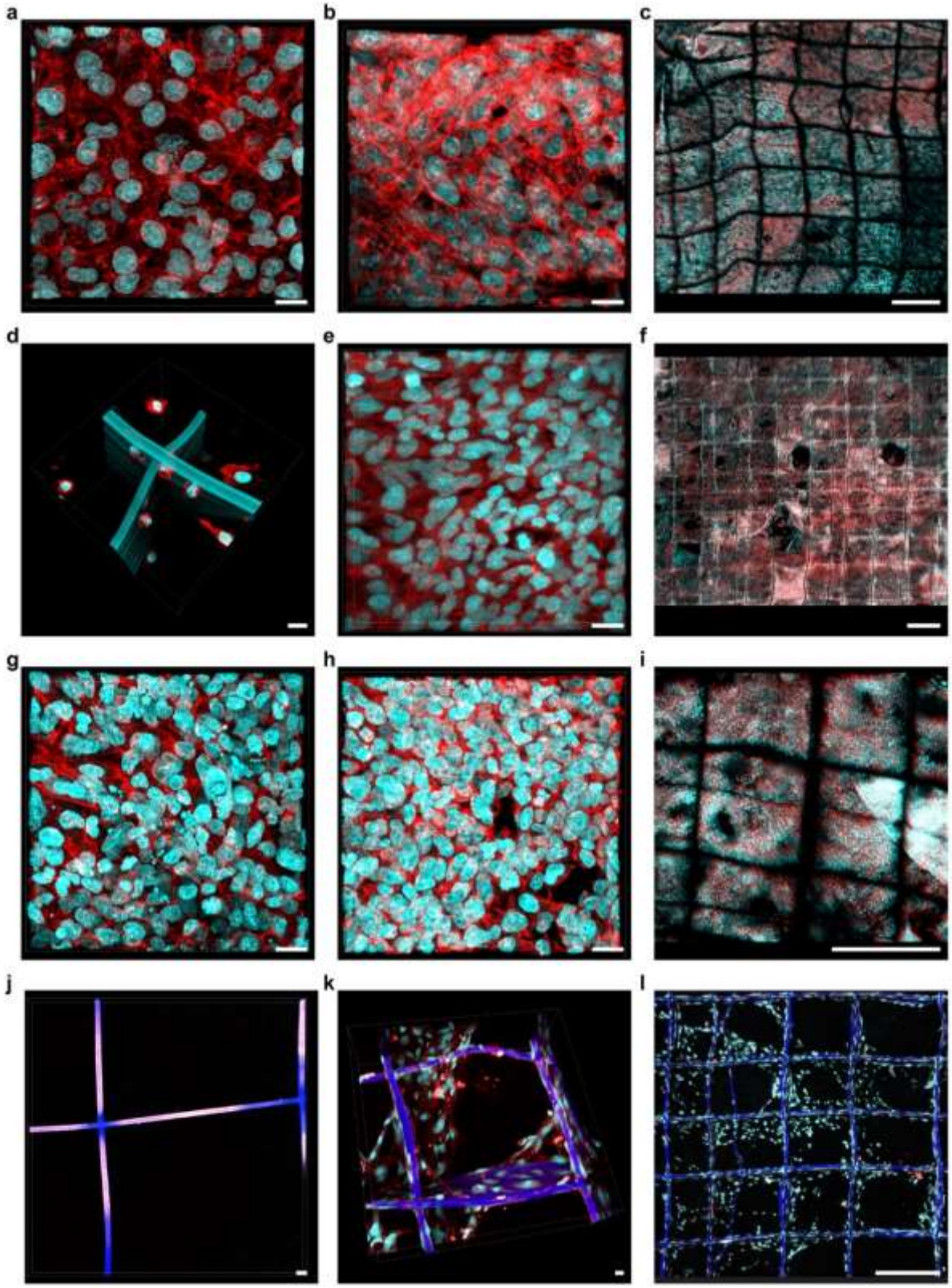

Figure S5. Suspended protein networks allow *in vitro* culture of a variety of cell types. (a-c) MDA-MB-231 breast cancer cells on suspended protein networks made from (a) collagen I and (b, c) fFn at day six of culture. (d-f) Sum159 breast cancer cells on fFn networks after (d) one day and (e, f) four days of culture. (g-i) Pancreatic cancer cells on fFn networks. (g) Pancreatic cancer cells from the UM53 epithelial patient-derived cell line after two-day culture. (h, i) ASPC1 mesenchymal pancreatic cancer cell line cultured four days. (j-l) Human umbilical vein endothelial cells cultured for seven days do not grow on suspended

protein networks composed of (j) laminin only but cells thrive well when (k, l) laminin and fFn are combined. Whereas cancer cells form confluent volumes across the large areas of the tessellated scaffold (c, f, i), HUVECS remain in lower density bridged structures as shown in (l). (a, b, d, e, g, h, j, k) Scale bars 25 μm. (c, f, i, l) Scale bars 500 μm. (a-l) Channels: cyan, cell nucleus; red, actin. (j-l) Channels: blue, tessellated scaffold; cyan, cell nucleus; red, actin.

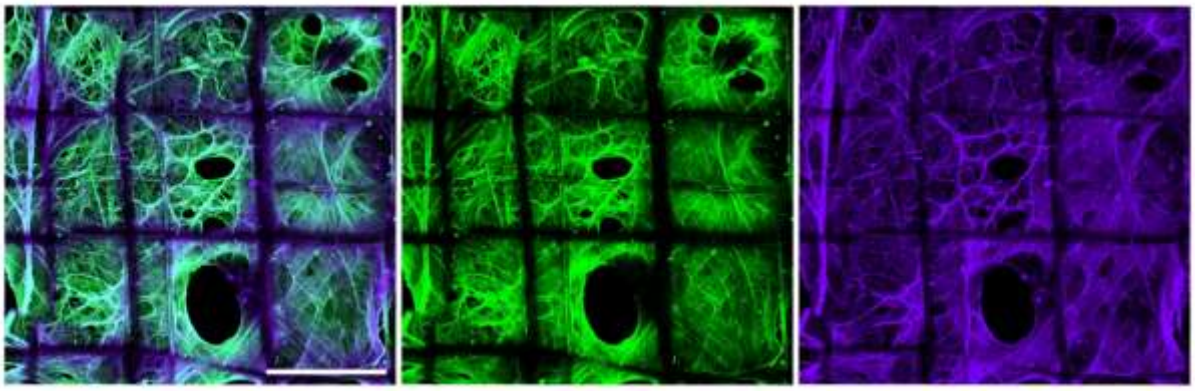

Figure S6. Large scale view of fFn network stained with Fn-3 Antibody. Split channel view detailing the presence of cellular fibronectin as recognized by the Fn-3 antibody across the open square pores and at large scale throughout the fFn network. Channels: green, fibronectin; purple, Fn-3 antibody. Scale bar 500 μm.

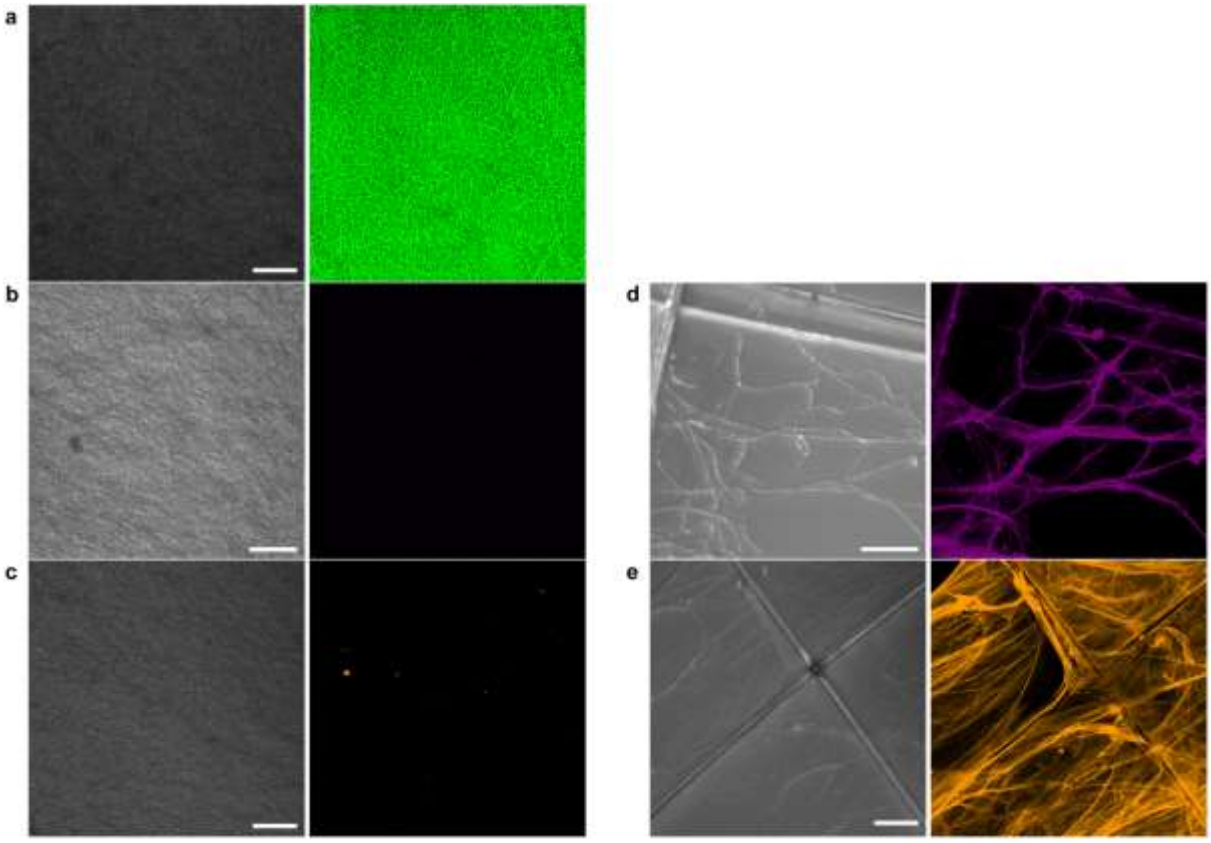

Figure S7. Hydrodynamically induced fibrillogenesis of fibronectin results in fFn that is recognized by IST-9 antibody. (a) *(right)* Fn (green) statically adsorbed onto a non-woven mat of PLGA fibers *(left)* also shown under brightfield. (b) *(right)* Fn-3 antibody staining (purple) of fibronectin conformally deposited onto a non-woven mat under the same procedure as *(a)*. Corresponding brightfield of Fn coated non-woven mat shown on the *left*. (c) *(left)* Non-woven mat with conformally deposited fibronectin by the same procedure as *(a)* with *(right)* antibody staining to identify EDA via IST-9 antibody staining (orange). (d) fFn network under brightfield *(left)* and with Fn-3 staining (purple) *(right)*. (e) fFn network under brightfield *(left)* and with IST-9 staining (orange) *(right)*. Both the Fn-3 and IST-9 antibody only stain positive on fFn networks but not conformally deposited Fn. Isotype controls support the results shown. All scale bars 100 μm.

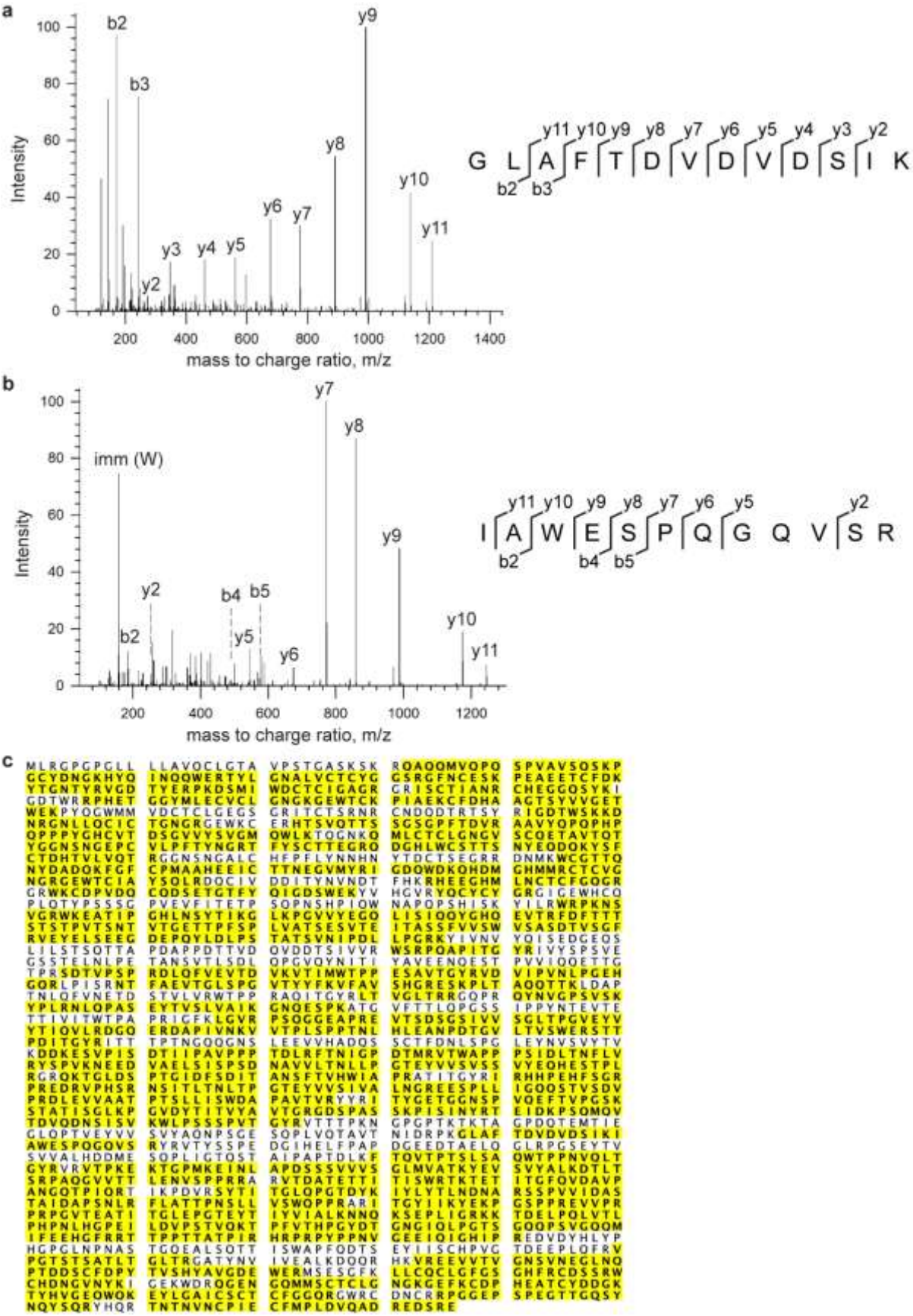

Figure S8. Proteomics analysis confirms presence of EDA sequence in fibronectin sourced for fFn networks. Two peptides unique to the alternatively spliced domain A (EDA) sequence were identified in the soluble fibronectin sourced for fFn network formation. Mass spectrometry results are shown for tryptic EDA peptides GLAFTDVDVDSIK and

IAWESPQGQVSR in *(a)* and *(b)* respectively. (a-b) N-terminus labelled as b ion and C-terminus labelled as y ion. (c) Sequence coverage map of fibronectin where yellow highlight indicates amino acid detection. At least 71% sequence coverage was reported. Sequence coverage may be greater than 71% and as high as 82%, if variable regions susceptible to modification during analysis are included.

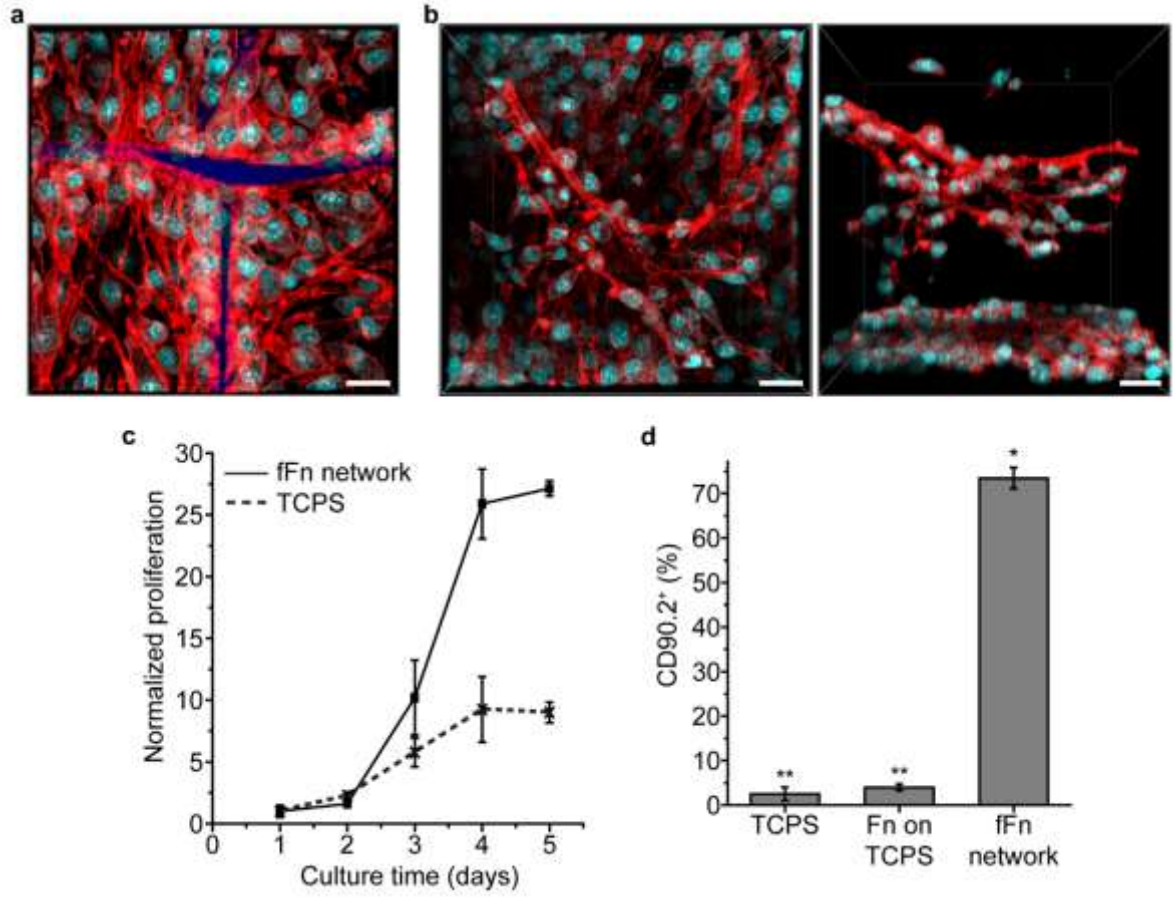

Figure S9. fFn networks promote a tumorigenic phenotype in AT-3 mouse breast cancer cells. (a) LSCM of AT-3 mouse breast cancer cells at the crosshair of the scaffold microfibers after three days of culture on fFn networks. (b) LSCM image after three days of culture showing *(left)* top view and *(right)* side view of the AT-3s forming multicellular structures as they span up into the open pore of the tessellated scaffold. (a-b) Channels: blue, tessellated scaffold; cyan, cell nucleus; red, actin. Scale bars 25 μm. (c) Growth curve for AT-3 cells cultured on TCPS (dotted line, crisscross marker) or fFn networks (solid line, square marker). (d) Quantification of the CD90.2^{+} population of AT-3 cells after three days of culture on TCPS, fibronectin conformally coated on TCPS (FN on TCPS), or fFn networks. Single star indicates that the fFn network result is statistically different from TCPS and FN on TCPS; double star indicates that TCPS and FN on TCPS results are statistically similar. $P<0.05$.

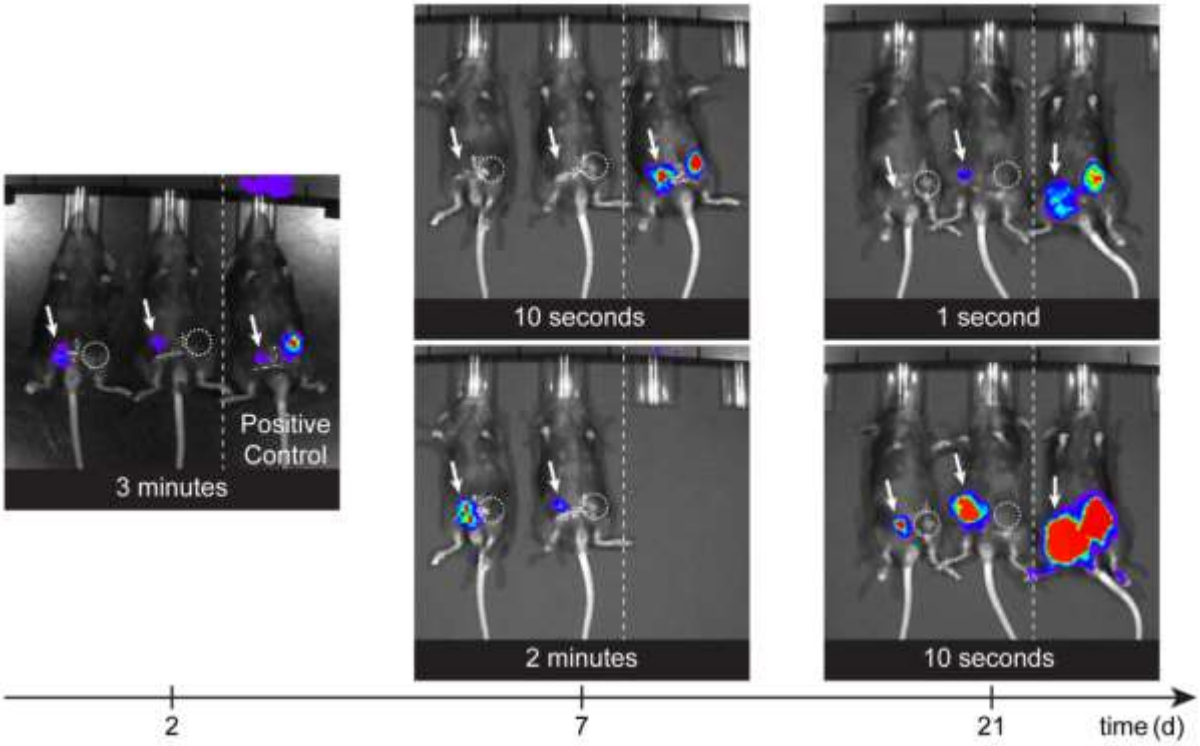

Figure S10. fFn networks show successful tumor engraftment in AT-3 mouse breast cancer model throughout the course of three weeks Bioluminescence image of immune-competent mice two, seven, and 21 days after orthotopic implantation of AT-3 cells. Four groups were examined: (1) 30,000 cells on three-millimeter-wide fFn network disks (2) 30,000 cells directly injected (3) 200,000 cells on a fFn network disk and (4) 200,000 cells directly injected as a positive control (being the minimum number of cells required to form a tumor by direct injection). The two mice on the left have group 1 in the left mammary fat pad as indicated by arrows and group 2 in the contralateral mammary fat pad on the right indicated by dashed circles. The third mouse on the right is a positive control carrying group 3 in the left mammary fat pad indicated by an arrow and group 4 in the contralateral right mammary fat pad. Exposure time for each bioluminescence image is indicated.

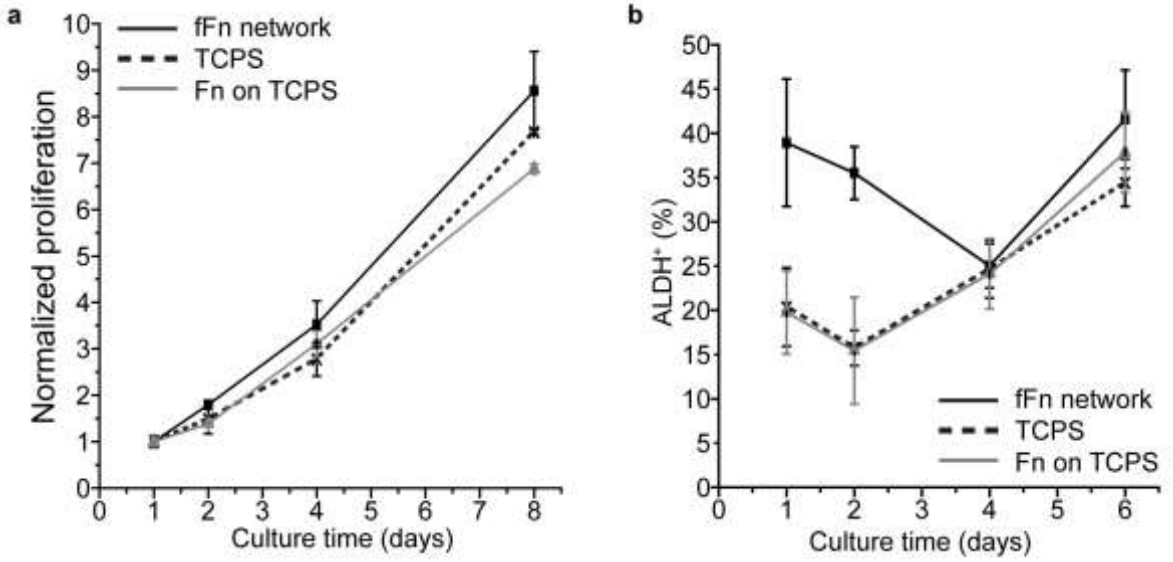

Figure S11. Proliferation trends and ALDH expression for MDA-MB-468 cells are similar across different cell culture substrates (a) Normalized proliferation measured by net mitochondrial activity of MDA-MB-468 cells shows little to no difference amongst fFn networks and control substrates despite observed changes in tumorigenicity. (b) Early timepoints show increased fractions of $ALDH^+$ (aldehyde dehydrogenase) cells on fFn networks relative to TCPS, and FN on TCPS, but ALDH populations across the three cell culture substrates converge and increase together from the fourth to sixth day in culture. (a-b) fFn networks (black solid line and square marker), TCPS (black dotted line and crisscross marker), and TCPS conformally coated with fibronectin or Fn on TCPS (grey line and triangular marker).

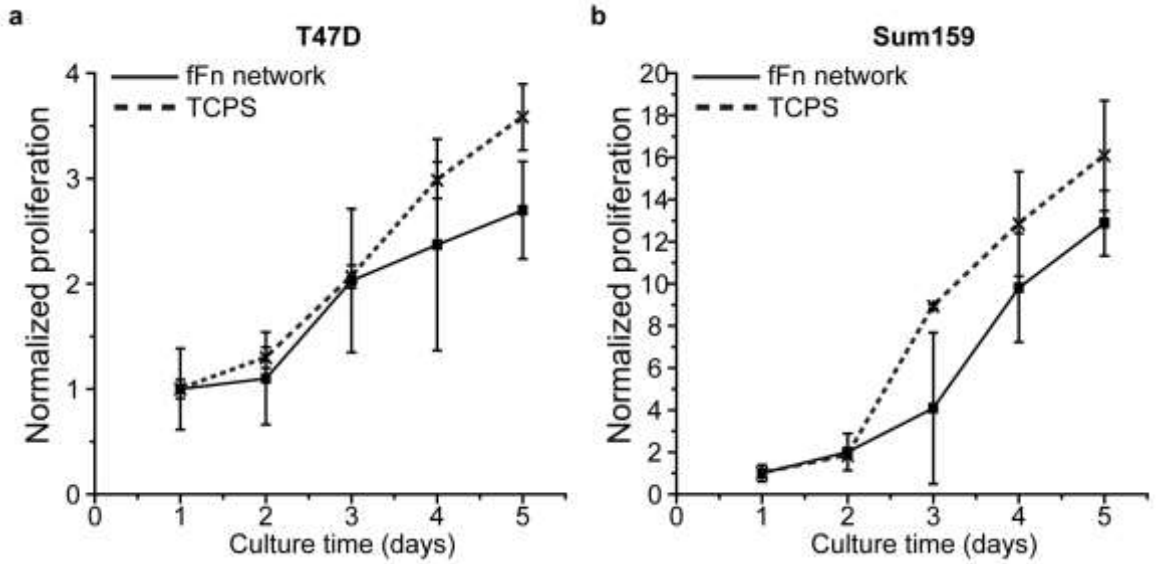

Figure S12. T47D and Sum159 human breast cancer cells proliferate on fFn networks fFn networks (black solid line and square marker) maintain similar proliferation trends as TCPS (black dotted line and crisscross marker) for (a) T47d and (b) Sum159 human breast cancer cell lines (as with MDA-MB-468s in *Supplementary Fig. 8a*). Normalized proliferation measured by luminescence gives fold increase in cell number over the course of a five-day culture.

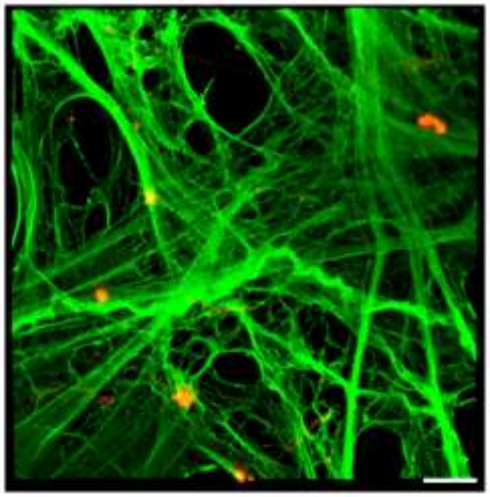

Figure S13. MDA-MB-468 human breast cancer cells secrete minimal amounts of laminin on fFn networks. After four days of culture, MDA-MB-468 cells were removed from the fFn network, and the remaining protein matrix was stained for fibronectin (green) and endogenously secreted laminin (orange). Scale bar 25 μm.

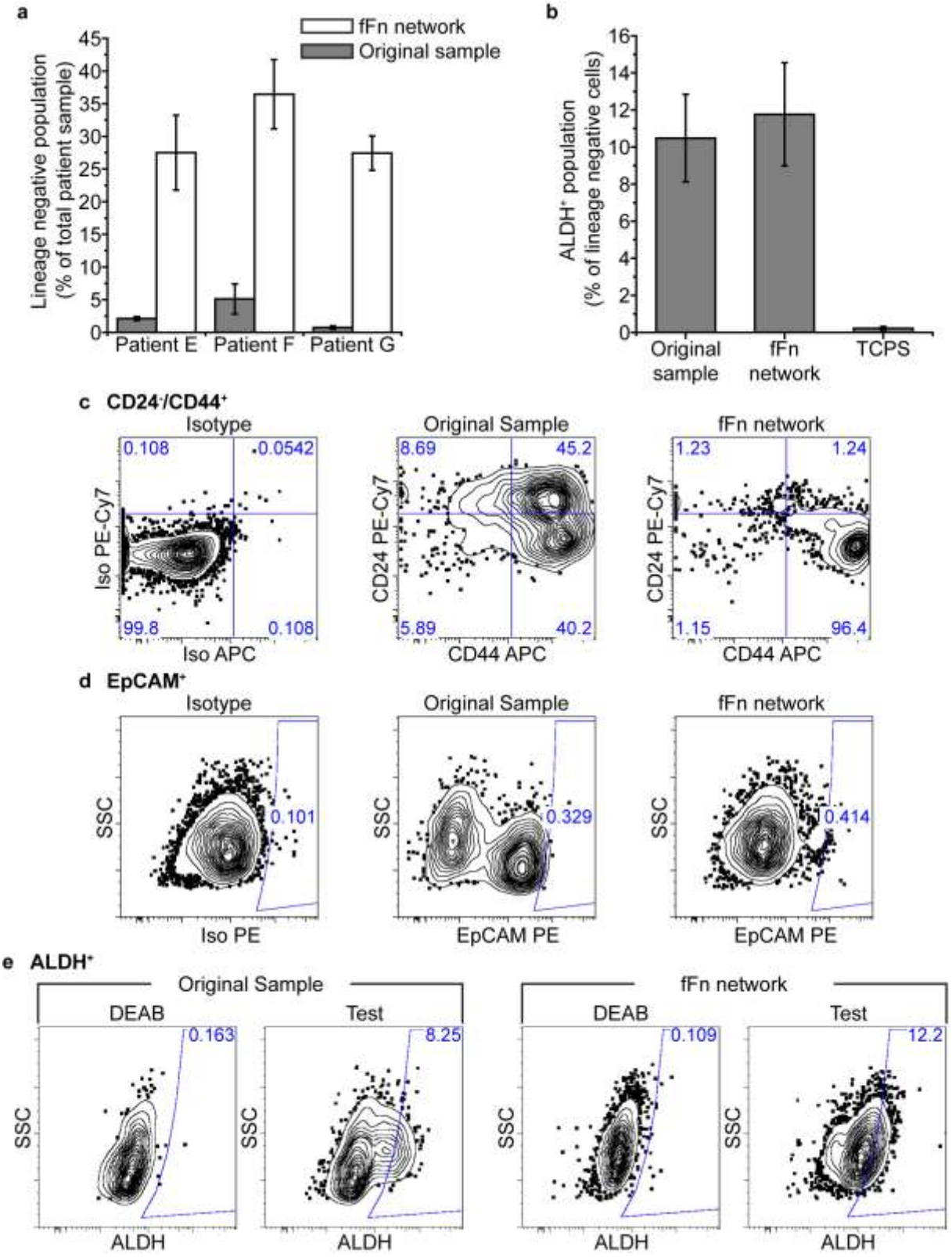

Figure S14. Six-day culture on fFn networks enriches breast cancer cell population in patient pleural effusion and ascites samples (a) Percent of total sample that are cancer cells indicated by the lineage negative population as measured directly from the patient (grey bars) and after six days of culture on fFn networks (white bars). (b) Percent of Patient E lineage negative cells that are $ALDH^+$ (aldehyde dehydrogenase) after culture on fFn networks or TCPS as compared to the original ascites sample. (c-e) Representative flow cytometry scatterplots for Patient E comparing the original ascites sample to cells cultured on fFn

networks for six days. The (c) $CD24^{-}/CD44^{+}$ (d) $EpCAM^{+}$ and (e) $ALDH^{+}$ cells within the lineage negative population were quantified.

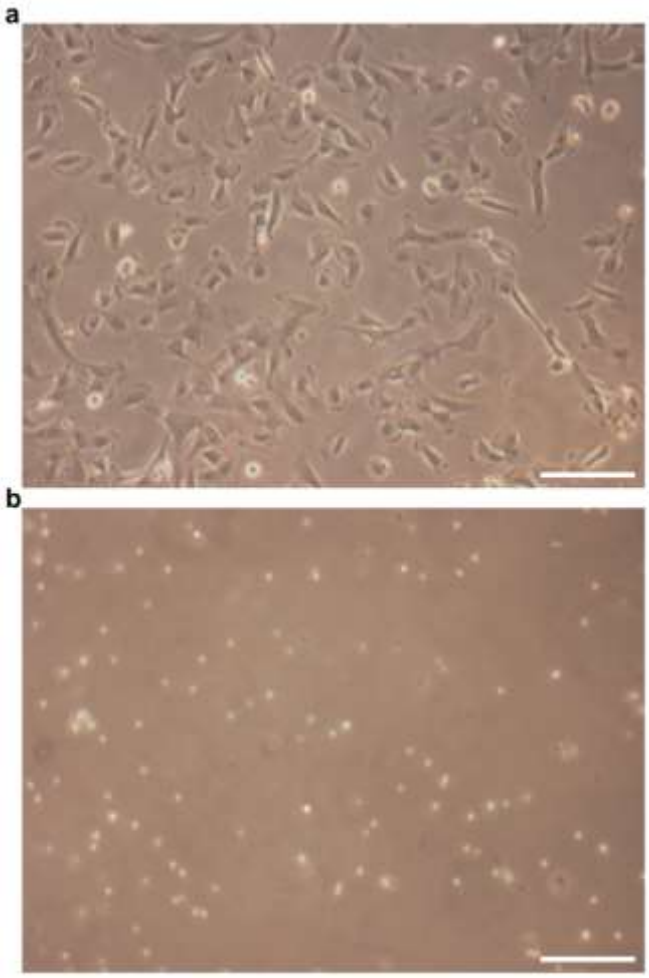

Figure S15. Patient ascites cells grow on tissue culture polystyrene if first expanded on fFn networks (a) Ascites sample from Patient E cultured first on fFn networks for two days then trypsinized and re-plated onto TCPS. (b) Brightfield microscope image of cells from the same patient sample in *(a)* plated directly from the patient onto TCPS. Image taken after one day of culture showing cells do not survive. Scale bars 25 μm.

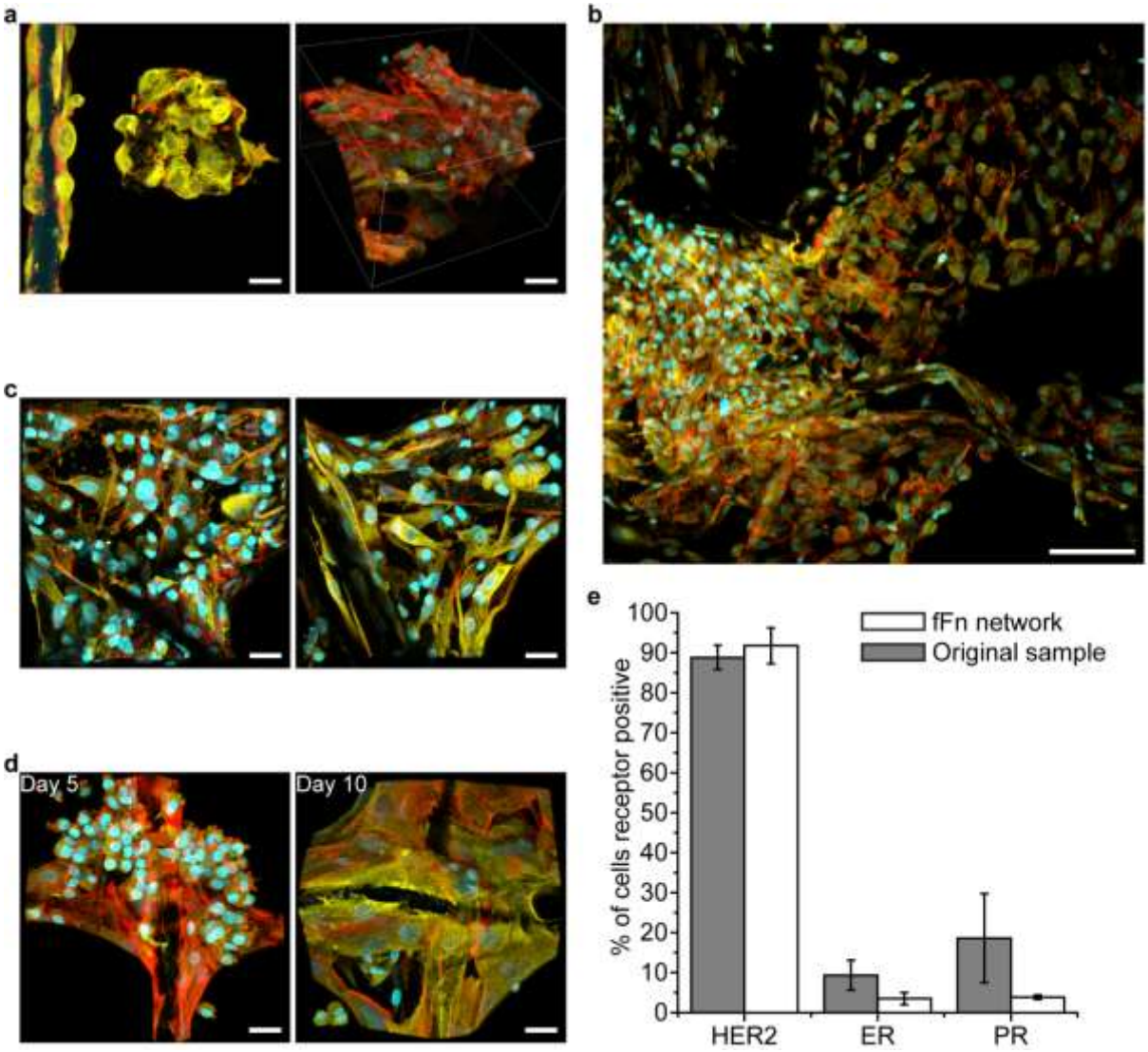

Figure S16. fFn networks provide a microenvironment for the expansion of patient pleural effusion and ascites samples *ex vivo* while maintaining receptor status (a-c) Pleural effusion samples from (a-b) Patient I and (c) Patient H cultured on fFn networks and imaged via LSCM showing heterogeneity, scalability, formation of 3D cell structures, and separation of cells by cell type into different areas of the same scaffold. (d) Population shifts in favor of cancer cells marked by cytokeratin in ascites sample from Patient J as the culture is carried out from five days to ten days on fFn networks. Representative LSCM images taken at the microfiber crosshair of the tessellated scaffold. (a-d) Channels: cyan, cell nucleus; red, actin; yellow, cytokeratin 5. Scale bar (a, c, d) 25 μm, (b) 100 μm. (e) Pleural effusion sample from Patient F was made into a cytospin, stained, and quantified for positive signals of human epidermal growth factor receptor 2 (HER2), estrogen receptor (ER), and progesterone receptor (PR). This analysis was performed on cells from the original patient sample (grey bars) and after six days of culture on fFn networks (white bars). Hospital data reported that this patient's receptor status was $HER2^{+}ER^{-}PR^{-}$. Error bars represent standard deviation of % of receptor positive cells measured from three to four microscope fields of view.